CRYSTAL GROWTH & DESIGN
2007
VOL. 7, NO. 11
2276–2278

Controllable Synthesis of One-Dimensional Chinelike Superstructures of Homogeneous $Bi_{100-x}Sb_x$ Alloys via a Template-Free Electrodeposition

Bo Zhou,[†,‡] Xing-Hua Li,[†] and Jun-Jie Zhu*[,†]

Key Laboratory of Analytical Chemistry for Life Science (MOE), School of Chemistry and Chemical Engineering, Nanjing University, Nanjing 210093, P. R. China, and College of Chemistry and Environment Science, Nanjing Normal University, Nanjing, P. R. China

Received May 30, 2007; Revised Manuscript Received September 27, 2007

ABSTRACT: One-dimensional (1D) superstructures are attracting increasing interests because of their unique physical and chemical properties. In our work, 1D chinelike superstructures of homogeneous $Bi_{100-x}Sb_x$ ($x = 0$–100) alloys were synthesized in aqueous solutions via a template-free electrochemical route at room temperature. The cyclic voltammetric analysis and the X-ray diffraction (XRD) study proved that Bi^{III} and Sb^{III} can be coreduced as a homogeneous solid solution; the Bi/Sb ratio in the alloy was greatly correlated to that in the aqueous solution, while also being affected by the deposition potential. The structures of the products were characterized by transmission electron microscopy (TEM), scanning electron microscopy (SEM), high-resolution transmission electron microscopy (HRTEM), and selected area electron diffraction (SAED). These 1D chinelike superstructures consisted of orderly aligned subcrystallites with only slight orientational distortion. The formation of these 1D superstructures was affected mainly by the deposition potential, and as the deposition potential became less and less negative, the products changed gradually from fine dendrites to big 1D chinelike superstructures. The orientational distortion in the structure, which is the reason for the chinelike pattern, might enhance the phonon scattering at subcrystallite boundaries and thus reduce the thermoconductivity, resulting in the improvement of the thermoelectric property.

Formation of the ordered superstructures, especially in one-dimensional (1D) nanostructures, is one of the key topics of modern materials chemistry because of their unique properties and potentially exciting applications.[1–3] In the case of the thermoelectric applications, 1D superstructures are theoretically believed to be better in reducing phonon transport while keeping high electron mobility.[4] Template-based electrodeposition is a promising technique and has been used to synthesize the 1D nanostructures of important thermoelectric materials, such as $Bi_{1-x}Sb_x$ ($x = 0$–1) and $(Bi, Sb)_2(Te, Se)_3$.[5–7] However, there is no report on the template-free electrodeposition for 1D nanostructures, and the reports on the formation of 1D superstructure of the thermoelectric materials are still rare.[8]

The electrical structure and the transport properties of the $Bi_{100-x}Sb_x$ alloy depend strongly on its concentration, and the alloy with $x = 4$–22 is considered to be the best n-type materials for thermoelectric cooling at temperature ~100 K.[9] Some techniques have been used to fabricate Bi–Sb alloys.[5–8,10–13] Herein, we focus on a template-free electrodeposition for the fabrication of 1D superstructures of $Bi_{100-x}Sb_x$ alloys. The prepared products were homogeneous, composition-controllable, one-dimensional, and superstructured. It is believed that all these characters can greatly improve the thermoelectric property.[4,10–14] The method used is simple, fast, and template-free. The composition and the morphology of the products can be controlled by adjusting the composition of the electrolyte and the deposition potential.

The potentiostatic electrochemical deposition and the cyclic voltammetry analysis were carried out at room temperature in a three-electrode cell, using indium tin oxide (ITO)-coated glass as working electrode, platinum wire as counter electrode, and saturated calomel electrode as reference. Aqueous Bi^{III} solution (soln 1) and Sb^{III} solution (soln 6) contained 0.02 M $Bi(NO_3)_3 \cdot 5H_2O$ and $Na(SbO)C_4H_4O_6$, respectively, and 0.2 M disodium ethylene diamine tetraacetate (EDTA). Other electrolytes were obtained by mixing the above Bi^{III} solution and Sb^{III} solution in different volume ratios. For solns 2–5, the concentration ratios of $[Sb^{III}]$ to $([Bi^{III}]+[Sb^{III}])$ were 12.5, 25, 50, and 75%, respectively.

* Corresponding author. E-mail: jjzhu@netra.nju.edu.cn.
† Nanjing University.
‡ Nanjing Normal University.

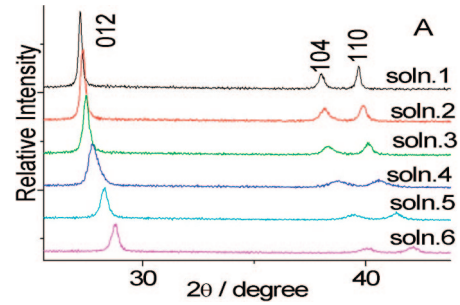

Figure 1. XRD patterns of the products deposited at −0.9V vs SCE in solution (soln) 1 ≈ soln 6.

The cyclic voltammetric analyses in Bi^{III} solution (soln 1) and Sb^{III} solution (soln 6) showed that the deposition potential of Sb was more negative than that of Bi, indicating that Sb^{III} was more difficult to be reduced than Bi^{III} in this condition.[15] However, for each of the mixed electrolytes (solns 2–5), there was only one reduction wave, indicating that Bi and Sb were coreduced as a solid solution. The observation of a single oxidation peak corresponding to the dissolution of the solid solution confirmed this deduction.[10–13]

The XRD results also confirmed this conclusion. Figure 1 shows the XRD patterns of the products deposited at −0.9V vs SCE. In solns 1 and 6, pure Bi and Sb were obtained. Their XRD patterns were indexed to the rhomb-centered hexagonal Bi (PDF 44-1246) and the isomorphic Sb (PDF 71-1173), respectively. The products obtained in solns 2–5 proved to be phase pure and isomorphic with Bi and Sb in crystalline structure. Each of their XRD patterns had a single set of diffraction peaks, which was set between those of pure Bi and pure Sb, and shifted to that of pure Sb as the concentration of Sb increased. It could be concluded that homogeneous $Bi_{100-x}Sb_x$ solid solutions were obtained. According to Vegard's law, [16] which is known to be followed by $Bi_{100-x}Sb_x$ solid solutions and assumes the linear relationship between the lattice parameters and the concentration of the solid solution, the percentages of Sb in the solid solutions deposited from soln 2 to soln 5 are respectively 8.8, 17, 38, and 70%, strongly correlated to but all a little smaller than the corresponding $[Sb^{III}]/([Bi^{III}]+[Sb^{III}])$ ratios

10.1021/cg0704955 CCC: $37.00
Published on Web 10/19/2007

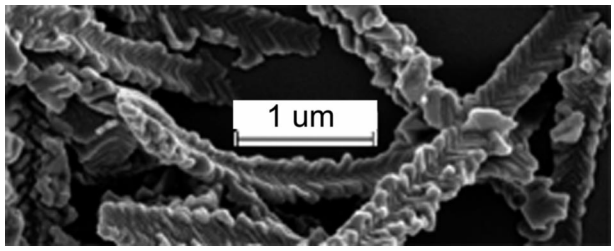

Figure 2. SEM image of the product deposited in soln 3 at −0.85 V vs SCE.

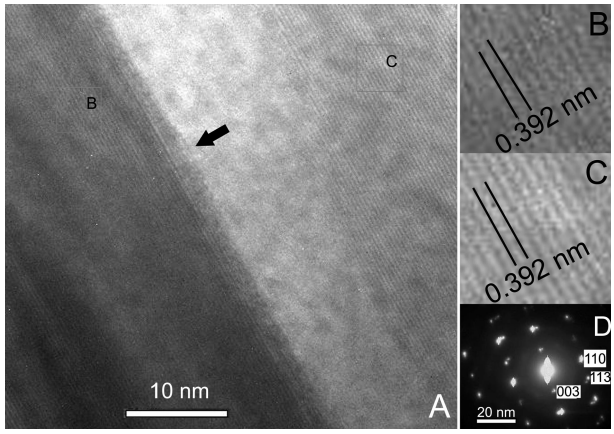

Figure 3. HRTEM images (A–C) and the SAED pattern (D) of the product deposited in solution 3 at −0.85 V vs SCE.

in solutions. This can be attributed to that the reduction of Sb^{III} is more difficult than that of Bi^{III}, as shown in the cyclic voltammgram. For the same reason, when the reduction of Sb^{III} was easier than that of Bi^{III}, as in the system reported by Besse,[17] the percentages of Sb in the solid solutions were larger than the corresponding $[Sb^{III}]/([Bi^{III}]+[Sb^{III}])$ ratios in solutions.

The composition of the alloy was also affected by the deposition potential. Comparing the XRD patterns of the products deposited at −0.9 and −1.3 V vs SCE, we observed that in the latter case, the diffraction peaks shifted more greatly to those of pure Sb and the Sb percentages in the alloys were calculated to be 11, 22, 47, and 72%, respectively, which were larger than in the former case and nearer to the corresponding $[Sb^{III}]/([Bi^{III}]+[Sb^{III}])$ ratios in solutions. This might be attributed to the fast deposition compensating to some degree for the difference between the reduction of Bi^{III} and Sb^{III}. On the other hand, less negative deposition potential, which means slower deposition, resulted in higher crystallinity, as indicated by the larger signal/noise ratio.

A less negative deposition potential resulted in the formation of 1D structures as observed in the SEM image shown in Figure 2. The 1D structures were 200–300 nm wide, several micrometers long, and chinelike superstructures which consisted of orderly aligned subcrystallites with a width of 20–30 nm and a length of ~100 nm.

More detailed study for the chinelike superstructures was carried out with HRTEM and SAED. In the HRTEM image of a "chine" shown in Figure 3, we can see well-crystallized subcrystallites with clear lattice fringes. The interplanar spacings are both ~0.39 nm, corresponding to the (003) lattice spacing of $Bi_{100-x}Sb_x$ alloy with $x \approx 15$. The crystallographic orientation of the subcrystallites is almost perfect. The bright diffraction spots in the SAED pattern shown in Figure 3D can be indexed, and the lattice parameter a is calculated to be ~0.451 nm, which is also in good agreement with what is expected for $Bi_{\sim 85}Sb_{\sim 15}$ alloy according to Vegard's law. However, there is a slight orientational distortion for the diffraction spots. Nevertheless, this result still confirms a high orientational

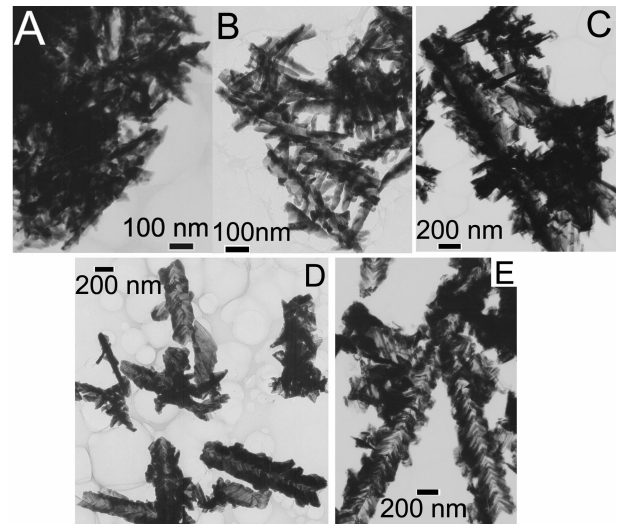

Figure 4. TEM images of the products deposited in solution 3 at various potentials. For A–E, the deposition potentials were −1.6, −1.3, −1.1, −0.9, and −0.85 V vs SCE, respectively.

order of the subunits in the superstructure.[18] This orientational distortion, which is the reason for the chinelike pattern, might result in the enhancement of the phonon scattering at the grain boundaries and the reducing of the thermal conductivity, and thus might improve the thermoelectric property.

Several nanoparticle-based formation mechanisms for the superstructures have been proposed, such as oriented attachment, surfactant-mediated aggregation, and a "brick-by-brick" aggregation mechanism.[19,20] In our work, the formation of the 1D superstructure was mainly affected by the deposition potential. The TEM images shown in Figure 4 indicated that the morphology of the products changed gradually from fine dendrites to bigger 1D chinelike superstructures as the potential became less and less negative. This suggested the following formation mechanism: In the electrodeposition, dendrites as a kind of skeletal crystals were preferentially obtained. When the deposition was performed fast at more negative potentials, a large amount of fine dendrites were obtained. However, when the deposition was performed slowly at less negative potentials, as the dendrites grew longer, there would be more time for the deposition to fill the spaces between the branches of the dendrites and to form the 1D chinelike superstructures. The exact reason for the remarkable orderliness of the nanocrystalline subunits, which resulted in diffraction patterns similar to those of single crystals, is still unknown, but tensorial polarization forces and dipole fields have been discussed.[21,22] In this electrodeposition, it is reasonable to suggest that the anisotropic electric field induced mutual ordering.[23]

In summary, 1D chinelike superstructures of homogeneous $Bi_{100-x}Sb_x$ ($x = 0$–100) alloys were synthesized in aqueous solutions via a template-free electrochemical route. The composition of the alloys was strongly correlated to the corresponding composition of the electrolytes and affected by the deposition potential. The morphology of the products was affected by the deposition potential and changed gradually from fine dendrites to bigger 1D chinelike superstructures as the potential became less and less negative. This method can be expected to be used in other systems.

Acknowledgment. We greatly appreciate the financial support of the European Commission Sixth Framework Program through a STREP grant to the SELECTNANO consortium, Contact 516992, and the National Natural Science Foundation of China for distinguished Young Scholars (20325516), the Key Program (20635020), and the Creative Research Group (20521503). B.Z. also thanks the Natural Science Foundation of the Jiangsu Higher Education

Institutions of China (Grant 06KJB150061) for support. The authors thank Professor Hong-Yuan Chen and Jian-Min Zhu for their kind help.

Supporting Information Available: Some experimental details, preparations of the samples for observation, XRD results, and cyclic voltammetry analyses (PDF). This information is available free of charge via the Internet at http://pubs.acs.org.

References

(1) Cölfen, H.; Antonietti, M. *Angew. Chem., Int. Ed.* **2005**, *44*, 5576–5591.
(2) Antonietti, M.; Ozin, G. *Chem.—Eur. J.* **2004**, *10*, 29–41.
(3) Murray, C. B.; Kagan, C. R.; Bawendi, M. G. *Science* **1995**, *270*, 1335–1338.
(4) Lin, Y. M.; Dresselhaus, M. S. *Phys. Rev. B* **2003**, *68*, 075304.
(5) Prieto, A. L.; Martín-González, M.; Keyani, J.; Gronsky, R.; Sands, T.; Stacy, A. M. *J. Am. Chem. Soc.* **2003**, *125*, 2388–2389.
(6) Martín-González, M.; Prieto, A. L.; Gronsky, R.; Sands, T.; Stacy, A. M. *Adv. Mater.* **2003**, *15*, 1003–1006.
(7) Menke, E. J.; Li, Q.; Penner, R. M. *Nano Lett.* **2004**, *4*, 2009–2014.
(8) Xue, F. H.; Fei, G. T.; Wu, B.; Cui, P.; Zhang, L. D. *J. Am. Chem. Soc.* **2005**, *127*, 15348–15349.
(9) Yamashita, O.; Tomiyoshi, S. *J. Appl. Phys.* **2002**, *92* (7), 3794–3802.
(10) Mallik, R. C.; Das, V. D. *Solid State Commun.* **2005**, *134* (3), 211–216.
(11) Devaux, X.; Brochin, F.; Dauscher, A.; Lenoir, B.; Martin-Lopez, R.; Scherrer, H.; Scherrer, S. *Nanostruct. Mater.* **1997**, *8*, 137–147.
(12) Cho, S. L.; Kim, Y.; Youn, S. J.; DiVenere, A.; Wong, G. K. L.; Freeman, A. J.; Ketterson, J. B.; Olafsen, L. J.; Vurgaftman, I.; Meyer, J. R.; Hoffman, C. A. *Phys. Rev. B* **2001**, *64* (23), 235330.
(13) Martín-González, M.; Prieto, A. L.; Knox, M. S.; Gronsky, R.; Sands, T.; Stacy, A. M. *Chem. Mater.* **2003**, *15* (8), 1676–1681.
(14) Patzke, G. R.; Krumeich, F.; Nesper, R. *Angew. Chem., Int. Ed.* **2002**, *41*, 2446–2461.
(15) Zhou, B.; Zhu, J. J. *J. Nanosci. Nanotechnol.* **2007**, *7* (2), 525–529.
(16) Berger, H.; Christ, B.; Troschke, J. *Cryst. Res. Technol.* **1982**, *17*, 1233–1239.
(17) Besse, F.; Boulanger, C.; Lecuire, J. M. *J. Appl. Electrochem.* **2000**, *30*, 385–392.
(18) Grassmann, O.; Neder, R. B.; Putnis, A.; LObmann, P. *Am. Mineral.* **2003**, *88*, 647–652.
(19) Penn, R. L.; Banfield, J. F. *Geochim. Cosmochim. Acta* **1999**, *63*, 1549–1557.
(20) Li, M.; Schnablegger, H.; Mann, S. *Nature* **1999**, *402*, 393–395.
(21) Busch, S.; Dolhaine, H.; DuChesne, A.; Heinz, S.; Hochrein, O.; Laeri, F.; Podebrad, O.; Vietze Weiland, T.; Kniep, R. *Eur. J. Inorg. Chem.* **1999**, *10*, 1643–1653.
(22) Wang, T. X.; Colfen, H.; Antonietti, M. *J. Am. Chem. Soc.* **2005**, *127*, 3246–3247.
(23) Agra, R.; Wijland, F.; Trizac, E. *Phys. Rev. Lett.* **2004**, *93*, 018301.

CG0704955